Longitudinal Hall Effect

LUDWIG GRABNER
International Business Machines Research Laboratory, Poughkeepsie, New York
(Received August 20, 1959)

The "Hall Field" is defined as the electric field which is an odd function of the magnetic field. Because of the Onsager relations it is perpendicular to the current. It is split into the conventional transverse Hall field (TH-field) in the direction of $\mathbf{B}\times\mathbf{I}$ and a longitudinal Hall field (LH-field) in the direction $\mathbf{I}\times(\mathbf{B}\times\mathbf{I})$. Some properties of the LH-field contrast with those of the TH-field. In particular, it vanishes (a) at saturation, (b) for spherical energy surfaces, and (c) when the magnetic field is parallel to an axis of rotation of the crystal. Its dependence on carrier concentration is the same as that of the TH-field; its sign, however, is determined by band structure as well as carrier sign. For a system consisting of n-type germanium the properties of the LH-field are investigated theoretically and experimentally.

I. INTRODUCTION

OHM'S law for an isothermal single crystal placed in a homogeneous magnetic field is[1]:

$$E_i=\rho_{ij}(\mathbf{B})I_j, \tag{1}$$

$\mathbf{E}$ is the electric field, $\mathbf{I}$ the current density and $\rho_{ij}(\mathbf{B})$ the resistivity tensor which is a function of the magnetic field $\mathbf{B}$.

If $\rho_{ij}(\mathbf{B})$ is written as the sum of a symmetric tensor $\tilde{\rho}_{ij}(\mathbf{B})$ and an antisymmetric tensor $\tilde{\rho}_{ij}(\mathbf{B})=\epsilon_{ijk}R_k(\mathbf{B})$ we have

$$E_i=[\tilde{\rho}_{ij}(\mathbf{B})+\epsilon_{ijk}R_k(\mathbf{B})]I_j, \tag{2}$$

where ϵ_{ijk} is the permutation tensor and $R_k(\mathbf{B})=\frac{1}{2}\epsilon_{ijk}\times\tilde{\rho}_{ij}(\mathbf{B})$ is the vector of the tensor $\tilde{\rho}_{ij}(\mathbf{B})$. $R(\mathbf{B})$ is an axial vector since $\tilde{\rho}_{ij}(\mathbf{B})$ is a polar tensor. Assuming the Onsager relations,[2] $\rho_{ij}(\mathbf{B})=\rho_{ji}(-\mathbf{B})$, Casimir[3] showed that $\tilde{\rho}_{ij}(\mathbf{B})$ is an even function of $\mathbf{B}$ and that $R(\mathbf{B})$, which he termed the Hall vector, is an odd function of $\mathbf{B}$. Measurements are usually made with respect to a laboratory reference frame, an orthogonal frame determined by $\mathbf{B}$ and $\mathbf{I}$ as shown in Fig. 1. Because of the Onsager relation the electric field E_I in the direction of the current is always even with respect to $\mathbf{B}$. Examples are transverse and longitudinal magnetoresistance. The electric field perpendicular to the current is composed of even and odd terms. The odd term $\tilde{E}$ will be called the Hall field in analogy with Casimir's terminology. Its components with respect to the laboratory frame, $\tilde{E}_{B\times I}$ and $\tilde{E}_{I\times(B\times I)}$, will be distinguished as transverse and longitudinal Hall fields (TH-field and LH-field) respectively. $\tilde{E}_{B\times I}$ is the field of interest in the conventional "Hall effect" measurement and the "Hall coefficient" is calculated from it in the usual way. The component of the electric field in the direction $\mathbf{I}\times(\mathbf{B}\times\mathbf{I})$ which is even in $\mathbf{B}$, i.e., $\tilde{E}_{I\times(B\times I)}$ is customarily called the "planar" Hall field.[4] The term "pseudo" Hall field has been used for $\tilde{E}_{I\times(B\times I)}+\tilde{E}_{I\times(B\times I)}$.[5] Clearly the LH-field $\tilde{E}_{I\times(B\times I)}$ and the "planar" Hall field investigated by Goldberg and Davis[4] are different. One is due to the antisymmetric tensor $\tilde{\rho}_{ij}(\mathbf{B})$ and reverses with $\mathbf{B}$, the other is due to the symmetric tensor $\tilde{\rho}_{ij}(\mathbf{B})$ and does not reverse with $\mathbf{B}$. The former is intimately connected with the Hall effect, the latter with magnetoresistance.

In Appendix A it is shown that the TH-field and the LH-field can be expressed as

$$\tilde{E}_{B\times I}=R_{I\times(B\times I)}(\mathbf{B})I, \tag{3}$$

$$\tilde{E}_{I\times(B\times I)}=-R_{B\times I}(\mathbf{B})I, \tag{4}$$

$R_{I\times(B\times I)}$ and $R_{B\times I}$ are projections of the Hall vector on unit vectors in the directions indicated and I is the magnitude of the current density. Thus once the directions of $\mathbf{B}$ and $\mathbf{B}\times\mathbf{I}$ are fixed the magnitude of the LH-field $\tilde{E}_{I\times(B\times I)}$ is independent of the angle between $\mathbf{B}$ and $\mathbf{I}$ which is not the case for the TH-field $\tilde{E}_{B\times I}$ as shown by Eq. (3) nor the planar Hall field

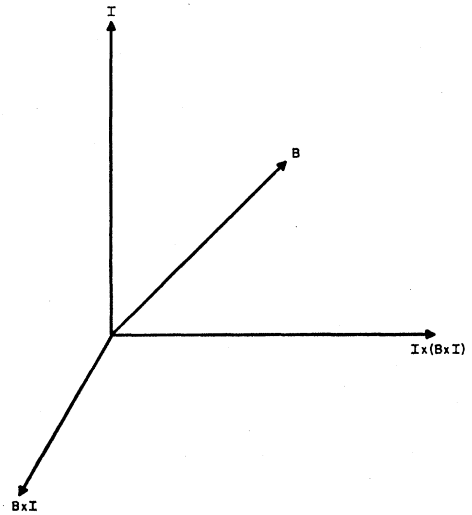

FIG. 1. Orthogonal "laboratory" reference frame constructed from $\mathbf{B}$ and $\mathbf{I}$: $\mathbf{I}$, $\mathbf{B}\times\mathbf{I}$, $\mathbf{I}\times(\mathbf{B}\times\mathbf{I})$.

[1] The summation convention of tensor analysis is used: if an index occurs twice summation is effected.
[2] L. Onsager, Phys. Rev. **37**, 405 (1931); **38**, 2265 (1931).
[3] H. B. G. Casimir, Revs. Modern Phys. **17**, 343 (1945).
[4] C. Goldberg and R. E. Davis, Phys. Rev. **94**, 1121 (1954).
[5] K. M. Koch, Z. Naturforsch. **10a**, 496 (1955).

$\bar{E}_{I\times(B\times I)}$ as shown by the analysis and experiment of Goldberg and Davis.

We will report on the measurement and interpretation of the LH-field in n-type germanium for the case that **B** is perpendicular to **I**, the usual arrangement in a Hall coefficient measurement. In that case the LH-field is parallel to the magnetic field and $\bar{E}_{I\times(B\times I)}$ becomes $\bar{E}_B$. Section II deals with the theory. First the phenomenological theory is given, then the transport theory, using the accepted many valley model of n-type germanium and a relaxation time that is a function of the energy but otherwise arbitrary. Section III discusses experimental techniques for measuring the LH-field and presents results:

II. THEORY

A. Phenomenological Theory

The existence of a point group symmetry for a single crystal simplifies the form of the resistivity tensor $\rho_{ij}(\mathbf{B})$ only for certain directions of **B**. The directions and simplifications are:

$\rho_{ij}(\mathbf{B}\|2\text{-fold axis})$

$$=\begin{bmatrix}\bar{\rho}_{11} & \bar{\rho}_{12} & 0\\ \bar{\rho}_{12} & \bar{\rho}_{22} & 0\\ 0 & 0 & \bar{\rho}_{33}\end{bmatrix}+\begin{bmatrix}0 & \bar{\rho}_{12} & 0\\ -\bar{\rho}_{12} & 0 & 0\\ 0 & 0 & 0\end{bmatrix}, \quad (5)$$

$\rho_{ij}(\mathbf{B}\|n(>2)\text{-fold axis})$

$$=\begin{bmatrix}\bar{\rho}_{11} & 0 & 0\\ 0 & \bar{\rho}_{11} & 0\\ 0 & 0 & \bar{\rho}_{33}\end{bmatrix}+\begin{bmatrix}0 & \bar{\rho}_{12} & 0\\ -\bar{\rho}_{12} & 0 & 0\\ 0 & 0 & 0\end{bmatrix}, \quad (6)$$

$\rho_{ij}(\mathbf{B}\perp 2n\text{-fold axis})$

$$=\begin{bmatrix}\bar{\rho}_{11} & 0 & 0\\ 0 & \bar{\rho}_{22} & \bar{\rho}_{23}\\ 0 & \bar{\rho}_{23} & \bar{\rho}_{33}\end{bmatrix}+\begin{bmatrix}0 & \bar{\rho}_{12} & \bar{\rho}_{13}\\ -\bar{\rho}_{12} & 0 & 0\\ -\bar{\rho}_{13} & 0 & 0\end{bmatrix}. \quad (7)$$

Since Eq. (1) is invariant with respect to an inversion a distinction between symmetry operations of the first sort and second sort need not be made. Therefore rotoinversion axes can be substituted for the pure rotation axes in Eqs. (5), (6), and (7). For example, Eq. (7) describes the resistivity if **B** is parallel to a plane of symmetry which is equivalent to a rotoinversion axis of order two. Equations (5), (6), and (7) are written in an orthogonal frame. In (5) and (6) x_3 is parallel to the axis of rotation, x_1 and x_2 arbitrary. In (7) x_1 is parallel to the axis of rotation, x_2 and x_3 arbitrary. If we assume that **I** is perpendicular to **B** and adopt a laboratory frame in which $x_1\|\mathbf{I}$ and $x_3\|\mathbf{B}$ then $\bar{E}_B(\mathbf{B}\perp 2n\text{-fold axis})=-\bar{\rho}_{13}I$ and $\bar{E}_B(\mathbf{B}\|n\text{-fold axis})=0$. Since $\bar{E}_B$ vanishes if **B** is parallel to an axis of rotation it cannot have an isotropic component. Equations (5) and (6) show that in that case the Hall vector is parallel to **B**.

If we expand (1) to first power in **B** in a standard reference frame[6] and then transform to a laboratory frame in which $\mathbf{I}\|1$-axis, $\mathbf{B}\|3$-axis we get:

$$E_i=\epsilon_{ijk}s_{kl}s_{mn}R_{ln}I_jB_m, \quad (8)$$

$\{s_{ik}\}$ is the transformation matrix and $R_{ln}=\partial R_l(\mathbf{B})/\partial B_n$. The form of R_{ln} for the point group symmetries in a standard frame is well known.[7] It is easily shown that $\bar{E}_B$ vanishes to first order only for point group symmetries belonging to the cubic system by writing out Eq. (8) and then taking into account the form which the point group symmetry imposes on R_{ln}. In the same way it can be shown that terms in $\bar{E}_B$ higher than the first in **B** need not vanish in any crystal system.

Mason, Hewitt, and Wick[8] expanded $\rho_{ij}(\mathbf{B})$ to terms including B^5 for a crystal of point group symmetry $[(4/m)\bar{3}(3/m)]$ (germanium) and determined E_I and $E_{B\times I}$ assuming $\mathbf{I}\perp\mathbf{B}$. From their analysis[9] we calculated $\bar{E}_B$:

$$\begin{aligned}\bar{E}_B=&(\gamma_{11}-3\gamma_{12})(l_2l_3^3+m_2m_3^3+n_2n_3^3)B^3I\\&+(\lambda_{111}-5\lambda_{112})(l_2l_3^5+m_2m_3^5+n_2n_3^5)B^5I\\&+(30\lambda_{123}-10\lambda_{112})(l_2l_3m_3^2n_3^2+m_2m_3l_3^2n_3^2\\&\qquad+n_2n_3l_3^2m_3^2)B^5I. \quad (9)\end{aligned}$$

From their results we give $\bar{E}_{B\times I}$ for comparison:

$$\begin{aligned}\bar{E}_{B\times I}=&(R_1+3\gamma_{12}B^2+5\lambda_{112}B^4)BI\\&-(\gamma_{11}-3\gamma_{12})(l_3^4+m_3^4+n_3^4)B^3I\\&-(\lambda_{111}-5\lambda_{112})(l_3^6+m_3^6+n_3^6)B^5I\\&-(90\lambda_{123}-30\lambda_{112})(l_3^2m_3^2n_3^2)B^5I. \quad (10)\end{aligned}$$

(l_1,m_1,n_1), (l_2,m_2,n_2), (l_3,m_3,n_3) are the direction cosines of **I**, $\mathbf{B}\times\mathbf{I}$ and **B**, respectively, with respect to the crystallographic frame of reference. R_i, γ_{ij}, λ_{ijk} are Mason, Hewitt, and Wick's abbreviations for R_{km}, γ_{kmno} and λ_{kmnopq} which are second, fourth, and sixth rank tensors defined by:

$$R_{km}=\frac{\partial R_k(\mathbf{B})}{\partial B_m}, \quad \gamma_{kmno}=\frac{1}{3!}\frac{\partial^3 R_k(\mathbf{B})}{\partial B_m\partial B_n\partial B_o},$$

$$\lambda_{kmnopq}=\frac{1}{5!}\frac{\partial^5 R_k(\mathbf{B})}{\partial B_m\partial B_n\partial B_o\partial B_p\partial B_q}$$

[6] We distinguish between three reference frames. (1) Crystallographic frame: in general not orthogonal and determined by the unit cell. (2) Standard frame: an orthogonal frame which has a fixed orientation with respect to the crystallographic frame. See "Standards on Piezoelectric Crystals, 1949." Proc. Inst. Radio Engrs. 37, 1378 (1949). (3) Laboratory frame.

[7] See, for example, J. F. Nye, *Physical Properties of Crystals* (Oxford University Press, 1957), p. 227.

[8] Mason, Hewitt, and Wick, J. Appl. Phys. 24. 166 (1953).

[9] The expression for the longitudinal field E_B including even terms is:

$$\begin{aligned}E_B=&(\alpha_{11}-\alpha_{12}-2\alpha_{66})(l_1l_3^3+m_1m_3^3+n_1n_3^3)B^2I+(\xi_{111}-\xi_{122}-4\xi_{442})\\&\times(l_1l_3^5+m_1m_3^5+n_1n_3^5)B^4I+(6\xi_{123}-6\xi_{112}+24\xi_{441}-4\xi_{442})\\&\times(l_1l_3m_3^2n_3^2+m_1m_3l_3^2n_3^2+n_1n_3l_3^2m_3^2)B^4I+(\gamma_{11}-3\gamma_{12})\\&\times(l_2l_3^3+m_2m_3^3+n_2n_3^3)B^3I+(\lambda_{111}-5\lambda_{112})(l_2l_3^5+m_2m_3^5\\&+n_2n_3^5)B^5I+(30\lambda_{123}-10\lambda_{112})(l_2l_3m_3^2n_3^2+m_2m_3l_3^2n_3^2\\&\qquad+n_2n_3l_3^2m_3^2)B^5I.\end{aligned}$$

For the definitions of α_{ik}, ξ_{ijk} see Mason, Hewitt, and Wick.

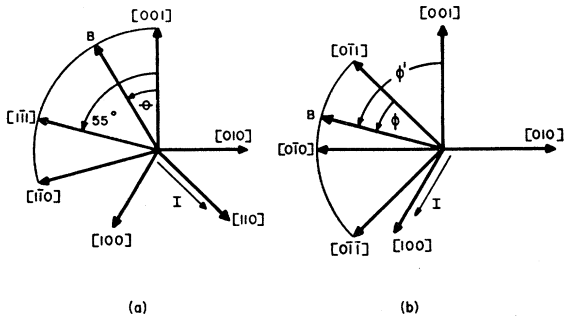

FIG. 2. Directions of **B** and **I** used in experiment relative to crystallographic axes. Magnetic field is moved in (110) and (100) planes in (a) and (b), respectively, through 90°. θ and ϕ are the angles measured in the experiment and their positive sense is shown.

in the crystallographic frame. R_i, γ_{ij}, and λ_{ijk} reduce to 1, 2, and 3 independent components, respectively, because of crystal symmetry.

Equation (9) agrees with our previous conclusions about the LH-field $\tilde{E}_B$: no isotropic term, zero if **B** is parallel to an axis of rotation, and absence of a first order term. The latter was shown to be a peculiarity of point symmetry groups belonging to the cubic system. It can be seen from Eq. (10) that the TH-field $\tilde{E}_{B\times I}$ has none of these properties.

In the experiment the following directions of **B** and **I** were selected:

Case *a*: **I** ∥ [110] direction, **B** in (110) plane.

Case *b*: **I** ∥ [100] direction, **B** in (100) plane.

as shown in Fig. 2 were the direction of **B** with respect to the crystallographic frame is specified by an angle θ (case *a*) and ϕ (case *b*) as measured in the experiment by a method to be described later. The positive sense of θ and ϕ is defined in Fig. 2.

It is convenient to label the LH-field $\tilde{E}_B{}^\theta$ or $\tilde{E}_B{}^\phi$ when the geometry is as in Fig. 2(a) or 2(b), respectively. In both cases the range 0°–90° is covered in the experiment. In addition to the symmetry relation discussed so far we have, for case *b*, $\tilde{E}_B{}^\phi(\phi)=-\tilde{E}_B{}^\phi(90°-\phi)$ for arbitrary magnetic fields as shown in Appendix B. Thus $\tilde{E}_B{}^\phi(\phi)$ must change sign at $\phi=45°$.

We summarize the restrictions which symmetry imposes on $\tilde{E}_B$ in the range 0°–90°. These restrictions are valid for *arbitrary magnetic fields*.

$$\tilde{E}_B{}^\theta(\theta)=0 \quad \text{when} \quad \theta=0°,\ 55°,\ 90°,$$
$$\tilde{E}_B{}^\phi(\phi)=0 \quad \text{when} \quad \phi=0°,\ 45°,\ 90°,$$
$$\tilde{E}_B{}^\phi(\phi)=-\tilde{E}_B{}^\phi(90°-\phi).$$

In addition, *to the order* B^5, Eq. (9) gives:

$$\tilde{E}_B{}^\theta=\tfrac{1}{4}\sin 2\theta(2-3\sin^2\theta)[(\lambda_{11}-3\lambda_{12})B^3+(\lambda_{111}-5\lambda_{112})B^5-(\lambda_{111}-15\lambda_{112}+30\lambda_{123})\tfrac{1}{2}\sin^2\theta B^5]I, \quad (11)$$

$$\tilde{E}_B{}^\phi=-\tfrac{1}{4}\sin 4\phi[(\lambda_{11}-3\lambda_{12})B^3+(\lambda_{111}-5\lambda_{112})B^5]I. \quad (12)$$

B. Transport Theory

For an ellipsoidal energy dependence on the crystal momentum the solution of the Boltzmann equation for an arbitrary magnetic field is[10]:

$$\mathbf{I}=-\tfrac{2}{3}e^2\Big[(\sum_v \sigma^{(1)}M^{-1})\mathbf{E}+(e/|M|c)\times(\sum_v \sigma^{(2)}M\mathbf{B})\times\mathbf{E}+\Big(\frac{1}{|M|}\Big)\Big(\frac{e}{c}\Big)^2\times(\sum \sigma^{(3)})\mathbf{B}\mathbf{B}\cdot\mathbf{E}\Big], \quad (13)$$

$$\sigma_{[ijk]}{}^{(n)}=\int \frac{(\partial f_0/\partial\epsilon)[\tau(\epsilon)]^n(d\mathbf{p})}{1+(e\tau/c)^2(M\mathbf{B}\cdot\mathbf{B}/|M|)}$$

is a scalar which for a rotational ellipsoid in the $[ijk]$ direction of crystal momentum space depends on the orientation through $M\mathbf{B}\cdot\mathbf{B}$. M is the effective mass tensor. The relaxation time $\tau(\epsilon)$ is assumed to be a function of the energy only but otherwise arbitrary. $\sum_v$ means summation over valleys which are rotational ellipsoids in equivalent [111] directions for *n*-type germanium. Equation (13) is evaluated for *n*-type germanium for cases (*a*) and (*b*) in Appendix C.

We define weak, intermediate and strong fields by $(e\tau/c)^2[(M\mathbf{B}\cdot\mathbf{B})/|M|]\ll,\sim,\gg 1$. The condition $\mu_H B \ll,\sim,\gg 1$ is approximately equivalent, μ_H being the Hall mobility. Neglecting $(e\tau/c)^2[(M\mathbf{B}\cdot\mathbf{B})/|M|]$ for weak fields we find $\tilde{E}_B=0$ For intermediate fields for which $(e\tau/c)^2[(M\mathbf{B}\cdot\mathbf{B})/|M|]<1$ the results to the order B^3 are:

$$\tilde{E}_B{}^\theta=R_0\Big(\frac{\mu_H B}{c}\Big)^2\sin 2\theta(2-3\sin^2\theta)\frac{2K+1}{6K}\times\Big(\frac{K-1}{K+2}\Big)^2\frac{\langle\epsilon\tau\rangle}{\langle\epsilon\tau^2\rangle^2}\Big[\langle\epsilon\tau^3\rangle-\frac{2K+1}{K+2}\frac{\langle\epsilon\tau\rangle\langle\epsilon\tau^4\rangle}{\langle\epsilon\tau^2\rangle}\Big]BI, \quad (14)$$

$$\tilde{E}_B{}^\phi=-R_0\Big(\frac{\mu_H B}{c}\Big)^2\sin 4\phi\frac{2K+1}{6K}\times\Big(\frac{K-1}{K+2}\Big)^2\frac{\langle\epsilon\tau\rangle}{\langle\epsilon\tau^2\rangle^2}\Big[\langle\epsilon\tau^3\rangle-\frac{2K+1}{K+2}\frac{\langle\epsilon\tau\rangle\langle\epsilon\tau^4\rangle}{\langle\epsilon\tau^2\rangle}\Big]BI, \quad (15)$$

$$R_0=3\frac{K(K+2)}{(2K+1)^2}\frac{\langle\epsilon\rangle\langle\epsilon\tau^2\rangle}{\langle\epsilon\tau\rangle^2}\frac{1}{nec}$$

is the "zero field" Hall coefficient, $K=m_{11}/m_\perp$,

$$\mu_H=\frac{e}{m_\perp}\frac{(K+2)}{(2K+1)}\cdot\frac{\langle\epsilon\tau^2\rangle}{\langle\epsilon\tau\rangle}$$

the Hall mobility $R_0\sigma$, and $\langle\epsilon\tau^n\rangle=\int f_0\epsilon\tau^n(d\mathbf{p})/\int f_0(d\mathbf{p})$.

[10] R. M. Broudy and J. M. Venables, Phys. Rev. **105**, 1757 (1957).

Equations (14) and (15) are the result of expanding Eqs. (16) and (17) of Appendix C to the order B^3 and then inverting the conductivity tensor $\mathcal{L}_{ij}(B)$ to obtain the resistivity tensor $\rho_{ij}(B)$. It is possible for the transport theory to yield results of higher symmetry than the phenomenological theory because of the model. An example of this are the phenomenological Seitz coefficients[11] which describe magnetoresistance to the order B^2 in a cubic material. The model imposes relations between the Seitz coefficients.[12] A comparison of Eqs. (11), (12), with (14) and (15) show that this is not the case for the LH-field $\tilde{E}_B$ at least to the order B^3.

The TH-field $\tilde{E}_{B\times I}$ increases monotonically with **B** and at saturation becomes a linear function of **B** independent of the band structure and scattering mechanism.[13] $\tilde{E}_{B\times I}$ is the electric field that stops current flow in the direction $\mathbf{B}\times\mathbf{I}$ due to the Lorentz force on the charge carriers. This is the mechanism that permits $\tilde{E}_{B\times I}$ to increase monotonically with **B**. The LH-field $\tilde{E}_B$, on the other hand, must be bounded since there is no force on the charge carriers in the direction of B due to the magnetic field. If we assume that the distribution function can be expanded in powers of $1/B$ for large magnetic fields[13] then $\tilde{E}_B \to 0$ as $B \to \infty$.

In obtaining numerical results from Eqs. (14) and (15) the approximation under which they were derived must be kept in mind: $(e\tau/c)^2[(M\mathbf{B}\cdot\mathbf{B})/|M|]<1$. Thus we cannot neglect ionized impurity scattering even if lattice scattering predominates since τ_L becomes large for small energies. Figure 3 shows the factor

$$\frac{2K+1}{6K}\left(\frac{K-1}{K+2}\right)^2\frac{\langle\epsilon\tau\rangle}{\langle\epsilon\tau^2\rangle^2}\left[\langle\epsilon\tau^3\rangle-\frac{2K+1}{K+2}\frac{\langle\epsilon\tau\rangle\langle\epsilon\tau^4\rangle}{\langle\epsilon\tau^2\rangle}\right]$$

versus $\dfrac{\mu_L}{\mu_L+\mu_I}$

the ratio of total mobility to ionized impurity mobility for $K=17$ and 20. The transport integrals were evaluated numerically using the approximation $\tau_L=\alpha\epsilon^{-\frac{1}{2}}$ and $\tau_I=\beta\epsilon^{+\frac{3}{2}}$ for the relaxation times for lattice scattering and ionized impurity scattering, respectively, $\alpha/\beta=6(\mu_L/\mu_I)$. The assumption of an isotropic relaxation time for τ_I for constant energy surfaces as anisotropic as those of n-type germanium was made to facilitate the calculations and becomes poorer as the amount of impurity scattering increases. Figure 4 shows the same factor as a function of K for $\mu_L/(\mu_L+\mu_I)$ equal to 0.5% and 3% and demonstrates that the sign of the LH-field is a function of band structure which is not the case for the TH-field: prolate and oblate spheroids give opposite signs.

[11] F. Seitz, Phys. Rev. **79**, 372 (1950).
[12] B. Abeles and S. Meiboom, Phys. Rev. **95**, 31 (1954).
[13] J. A. Swanson, Phys. Rev. **99**, 1799 (1955).

III. MEASUREMENTS

A. Experimental Details

The measurements were made on single crystal samples of n-type antimony-doped germanium oriented and cut as shown in Fig. 5. The sample was first oriented by x-ray analysis as a cube. A "3-dimensional cross" was then cut on a Do-All MTA-6 precision slicing machine. The carrier concentration is 1.5×10^{15}/cm^3 determined from weak field Hall measurements by the approximation $R_0=1/nec$ on a bridge shaped[14] sample cut from the same ingot as the "3-dimensional cross." Three pairs of probes were soldered to the sample, the solder wetting the whole 1.5×1.5 mm^2 surface. One pair of probes served as current leads, the other two as potential probes. The magnetic field is in the plane of the two potential probes. The sample is fixed in a tube to which helium is admitted as a thermal exchange gas after evacuation. The tube can be rotated through 360° and is immersed in a Dewar flask containing liquid nitrogen for the 77°K runs or a dry ice-alcohol mixture for the 200°K runs. A 12-in. Varian magnet provided uniform fields up to 20 000 gauss which were measured with a nuclear resonance magnetometer. Sample current and potentials were measured with a potentiometer galvanometer setup. The four voltages obtained by reversing separately the current and magnetic field are averaged so as to eliminate even functions of **I** and **B**.

It is shown in Appendix D how the angles θ and ϕ (see Fig. 2) and $\tilde{V}_B$ and $\tilde{V}_{B\times I}$ are determined from the potential probe measurements $\tilde{V}_{P_1}$ and $\tilde{V}_{P_2}$. A precise determination of θ and ϕ is essential to the calculation of $\tilde{V}_B$ from $\tilde{V}_{P_1}$ and $\tilde{V}_{P_2}$ because $\tilde{V}_B/\tilde{V}_{B\times I}\sim1/100$ and hence it is difficult to separate $\tilde{V}_B$ from $\tilde{V}_{B\times I}$. The method used allowed a determination of θ and ϕ to a precision $\sim0.1°$.

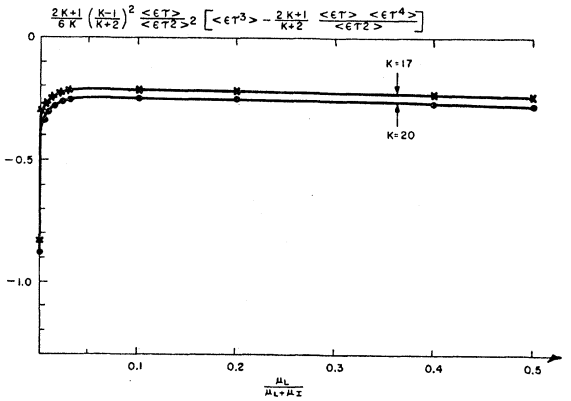

FIG. 3. The factor

$$\frac{(2K+1)}{6K}\left(\frac{K-1}{K+2}\right)^2\frac{\langle\epsilon\tau\rangle}{\langle\epsilon\tau^2\rangle^2}\left[\langle\epsilon\tau^3\rangle-\frac{2K+1}{K+2}\frac{\langle\epsilon\tau\rangle\langle\epsilon\tau^4\rangle}{\langle\epsilon\tau^2\rangle}\right]$$

of Eqs. (14) and (15) *versus* $\mu_L/(\mu_L+\mu_I)$ for $K=20$ and $K=17$ assuming lattice scattering and ionized impurity scattering.

[14] P. P. Debye and E. M. Conwell, Phys. Rev. **93**, 693 (1954).

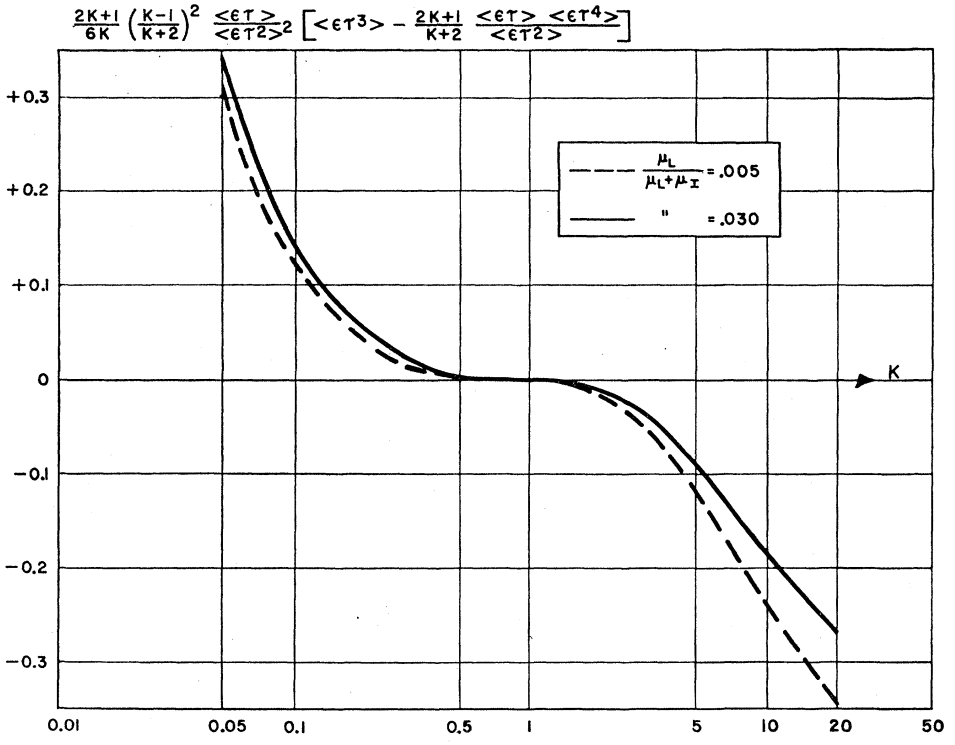

FIG. 4. The same factor plotted in Fig. 4 *versus* mass ratio K when $\mu_L/(\mu_L+\mu_I)$ is 0.5% or 3%.

Galvanomagnetic measurements are usually made on long thin samples in which the potential probe contacts are point contacts in order to avoid troublesome correction factors which are a function of the geometry and the magnetic field. For plane samples differing from the long thin ideal correction factors are discussed in the literature.[15–19] However, our geometry is not plane, nor are the potential probe contacts point contacts. We know no way of reducing the voltage $\tilde{V}_B$ to an electric field $\tilde{E}_B$ because of the complexity of our sample geometry. For our purposes this is unimportant since we are concerned with contrasting the properties of the LH-field with the TH-field, for which a relative measurement suffices. The "3-dimensional cross" sample geometry was chosen because it is obviously convenient for the measurements we intended. Its validity is justified experimentally, i.e., if $\tilde{V}_B$ fulfills the symmetry restrictions on the LH-field $\tilde{E}_B$ we identify it with the latter except for a geometrical factor which is unknown because of the complexity of the sample geometry.

B. Results and Discussion

1. Data at 200°K

Figure 6 shows typical data of $\tilde{V}_B$ *versus* B with θ and ϕ as parameters. Figure 7 is a replot of Fig. 6 showing $\tilde{V}_B/B^3$ *versus* B^2 which, in the range of validity of Eqs. (11) and (12), should be linear. This is seen to extend to 6 kilogauss. The intercepts and slopes of the linear portion give values consistent with the angular dependence demanded by Eqs. (11) and (12).

An analysis of the data shows that up to 4 kilogauss the error made by neglecting the B^5 term is small (<10%). Therefore, if $B=4$ kilogauss, $\tilde{V}_B{}^\theta$ *versus* θ should vary as the $\sin 2\theta(2-3\sin^2\theta)$ according to Eq. (11).

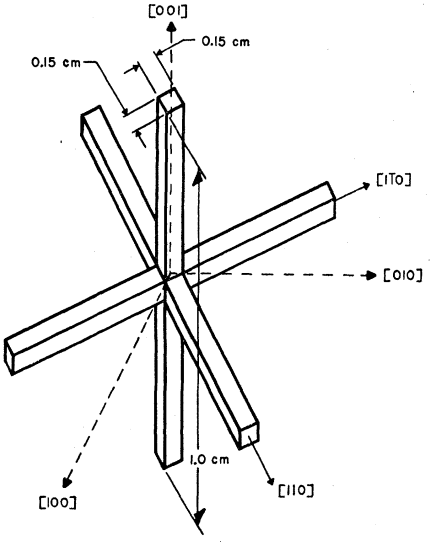

FIG. 5. "3-dimensional cross." Sample geometry used in experiment and its relation to crystallographic axes.

[15] Isenberg, Russel, and Greene, Rev. Sci. Instr. **19**, 685 (1948).
[16] J. Volger, Phys. Rev. **79**, 1023 (1950).
[17] R. F. Wick, J. Appl. Phys. **25**, 741 (1954).
[18] F. Kuhrt, Siemens-Z. **28**, 370 (1954).
[19] H. J. Lipmann and F. Kuhrt, Z. Naturforsch. **13a**, 462, 474 (1958).

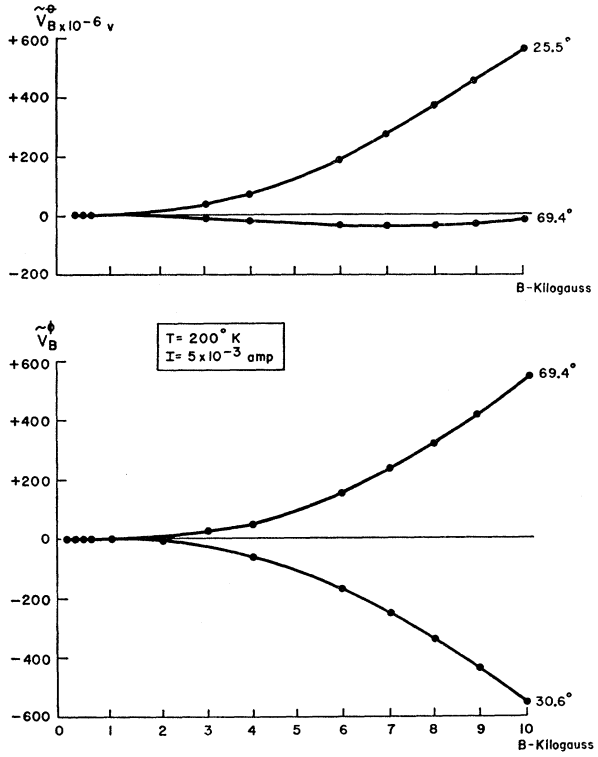

FIG. 6. LH-voltage *versus* magnetic field with θ and ϕ as parameters.

$\tilde{V}_B{}^{\phi}$ *versus* ϕ should vary as $-\sin4\phi$ up to $B=6$ kilogauss according to Eq. (12). Figure 8 shows V_B (4 kilogauss)

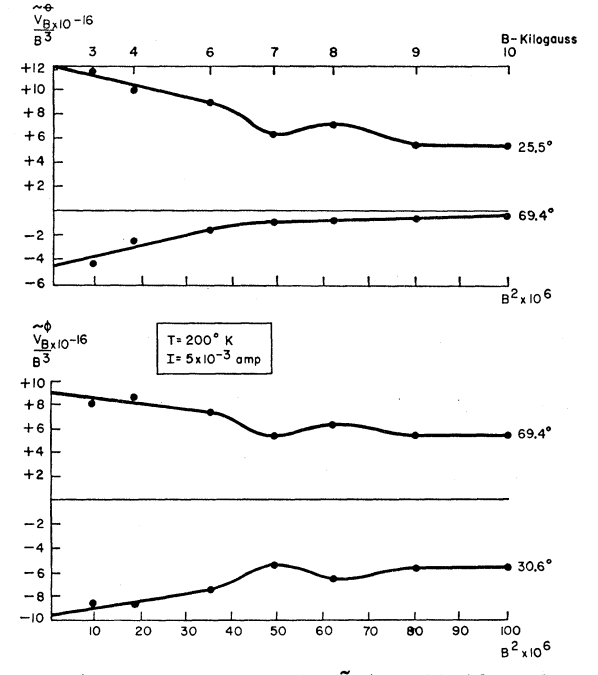

FIG. 7. Replot of Fig. 6 showing $\tilde{V}_B/B^3$ *vs* B^2 with θ and ϕ, respectively, as parameters.

versus θ and ϕ, respectively. Experimental values are plotted as points, the curves are $\sin2\theta(2-3\sin^2\theta)$ and $-\sin4\phi$ normalized to give the best fit. The experimental data is seen to be in good agreement with the phenomenological theory represented by Eqs. (11) and (12). Deviations from the theoretical solid curves are probably due to small misalignments in the cutting of the sample.

In order to give an idea of the relative value of the LH-field with respect to the TH-field Fig. 9 shows $\tilde{V}_B{}^{\phi}/\tilde{V}_{B\times I}{}^{\phi}$ *versus* B for $\phi=30.6°$ at which angle the largest LH-voltages were observed. The consistency of the data of this experiment supports the assumption that the correction factors for the geometry of the

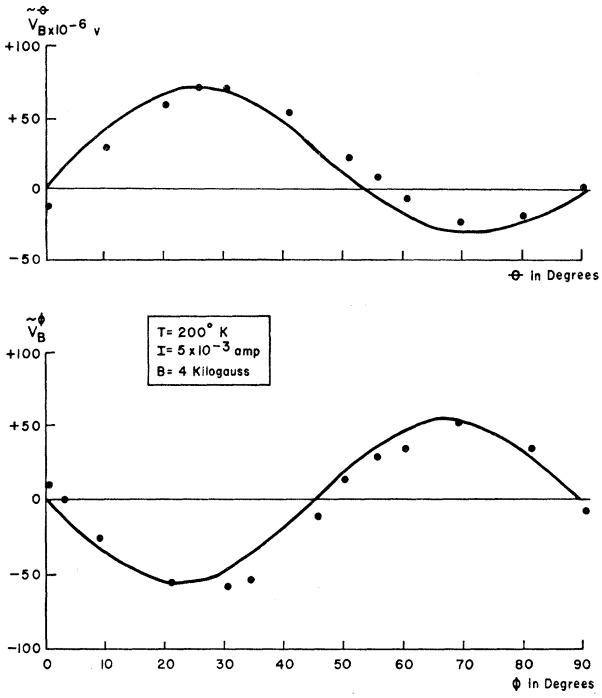

FIG. 8. Angular dependence of the LH-voltage at a magnetic field of 4 kilogauss. Curves are $\sin2\theta(2-3\sin^2\theta)$ and $-\sin4\phi$ normalized to give the best fit.

sample are identical for both arms, hence $\tilde{V}_B{}^{\phi}/\tilde{V}_{B\times I}{}^{\phi}=\tilde{E}_B{}^{\phi}/\tilde{E}_{B\times I}{}^{\phi}=-R_{B\times I}/R_B$ according to Eqs. (3) and (4). Since the Hall vector is perpendicular to **I** when **B** is in a plane of symmetry [see Eq. (7)] we conclude from Fig. 9 that it is almost parallel to the magnetic field for fields up to 10 kilogauss. To give an idea of the ratio of the LH-field to the TH-field predicted by theory we calculate $\tilde{E}_B{}^{\phi}/\tilde{E}_{B\times I}{}^{\phi}=+0.016$ when $\phi=30.6°$ and $B=4$ kilogauss. This calculation uses Eq. (15), the satisfactory approximation $\tilde{E}_{B\times I}=R_0BI$, the measured value of $\mu_H=6.5\times10^3$ cm²/v-sec and a value of -0.27 for the factor shown in Fig. 3 corresponding to $K=20$ and $\mu_L/(\mu_L+\mu_I)=0.03$. The latter is estimated from the Conwell-Weisskopf[20] formula for ionized impurity

[20] E. Conwell and V. F. Weisskopf, Phys. Rev. **77**, 388 (1950).

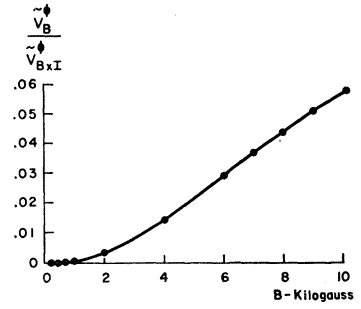

FIG. 9. Ratio of LH-voltage to TH-voltage *versus* magnetic field. $\phi=30.6°$, $T=200°$K.

mobility in conjunction with the estimate of impurity concentration given previously, and the empirical formula for lattice scattering mobility for n-type Ge due to Morin and Maita.[21] Experimentally we find $\tilde{V}_{B^\phi}/\tilde{V}_{B\times I^\phi}=+0.014$ (see Fig. 9).

2. *Data at* 77°K

At 77°K the Hall mobility μ_H is three times larger than at 200°K. At 10 kilogauss, for example, $\mu_H(200°\text{K})\times B=0.7$ and $\mu_H(77°\text{K})B=2$. Hence Fig. 10 which shows $\tilde{V}_B$ *versus* B with θ and ϕ as parameters can be expected to reveal strong field characteristics of $\tilde{V}_B$, *viz.*, a nonmonotonic behavior with respect to magnetic field in contrast to the TH-field which increases monotonically with B. It can be seen that we are far from saturation where the LH-field is expected to vanish.

Figure 11 shows $\tilde{V}_B$ (11 kilogauss) *versus* θ and ϕ, respectively, and demonstrates the symmetry relations demanded by the phenomenological theory: vanishing of $\tilde{V}_B$ when **B** is parallel to a rotational axis and $\tilde{V}_{B^\phi}(\phi)-\tilde{V}_{B^\phi}(90°-\phi)$. The curve drawn in $\tilde{V}_{B^\phi}$ (11 kilogauss) *versus* ϕ is $-\sin4\phi$ normalized to give the best fit. The data shown for $\tilde{V}_{B^\phi}$ (11 kilogauss) *versus* ϕ is representative of that obtained when a magnetic field up to 20 kilogauss (the largest used in the experiment) is used as a parameter, i.e., $\tilde{V}_{B^\phi}(B)$ *vs* ϕ could always be fitted by $-\sin4\phi$ regardless of magnitude of field or temperature. This strongly suggests that the augular dependence of $\tilde{V}_{B^\phi}$ is $-\sin4\phi$ independent of the magnetic field. This does not contradict the weaker requirement $\tilde{V}_{B^\phi}(\phi)=-\tilde{V}_{B^\phi}(90°-\phi)$ and is certainly true of $\tilde{V}_{B^\phi}$ up to terms in B^5 as shown by Eq. (10).

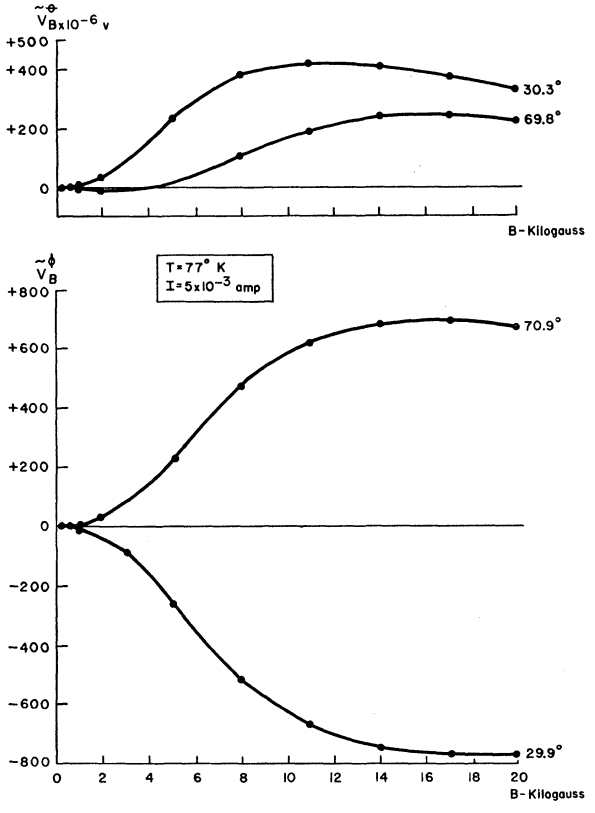

FIG. 10. LH-voltage *versus* magnetic field with θ and ϕ as parameters.

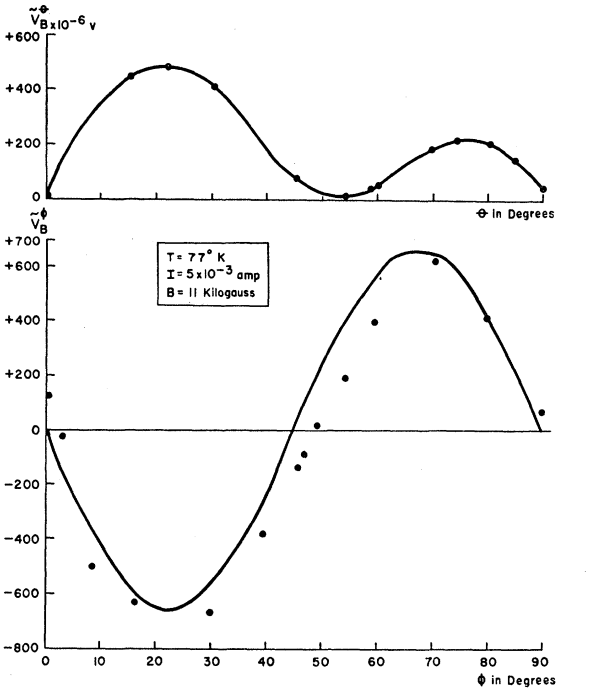

FIG. 11. Angular dependence of the LH-voltage for a magnetic field of 11 kilogauss. In $\tilde{V}_{B^\phi}$ *vs* ϕ the curve is $-\sin4\phi$ normalized to give the best fit.

Figure 12 shows $\tilde{V}_{B^\phi}/\tilde{V}_{B\times I^\phi}$ *versus* B when $\phi=29.9°$ at which angle we observed the largest LH-voltages. Comparison with Fig. 9 clearly shows the effect of saturation although neither the LH-field nor the TH-field are completely saturated. $\tilde{E}_B$ is seen to be small compared to $\tilde{E}_{B\times I}$. Since $\tilde{E}_B/\tilde{E}_{B\times I}=-R_{B\times I}/R_B$ the Hall vector is almost parallel to **B**. However, the magnitude of $\tilde{E}_B$ may be quite large for certain directions of the magnetic field especially if the sample is

[21] F. J. Morin and J. P. Maita, Phys. Rev. **94**, 1525 (1954).

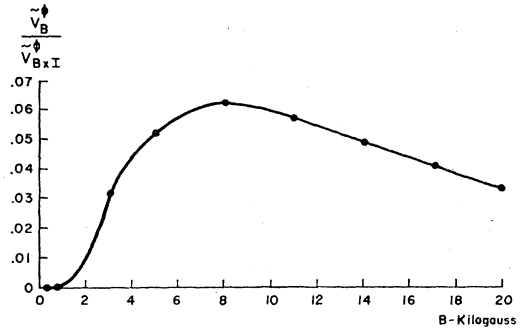

FIG. 12. Ratio of LH-voltage to TH-voltage *versus* magnetic field. $\phi=29.9°$, $T=77°$K.

pure enough since the LH-field has the same carrier concentration dependence as the TH-field. The LH-field was found very sensitive to inhomogeneities which revealed themselves by deviations from the symmetry relations. The choice of material with a carrier concentration of $1.5\times10^{15}/\text{cm}^3$ was made in order to avoid inhomogeneities. The presence of a LH-field excludes spherical energy surfaces; however, detailed deductions about the band structure and scattering are complicated by the fact that the LH-field is different from zero only for "intermediate" magnetic fields, a region in which expressions for the LH-field in terms of solutions of the Boltzmann equation are not simple.

IV. ACKNOWLEDGMENTS

The author wishes to express his indebtedness to B. J. Canavello whose services have been valuable in carrying out the experimental work and to J. A. Swanson and J. F. Woods for helpful conversations.

APPENDIX A

By definition the TH-field $\tilde{E}_{B\times I}$ and the LH-field $\tilde{E}_{I\times(B\times I)}$ are:

$$\tilde{E}_{B\times I}=\frac{(\mathbf{R}\times\mathbf{I})\cdot(\mathbf{B}\times\mathbf{I})}{BI\sin\gamma},\quad \tilde{E}_{I\times(B\times I)}=\frac{(\mathbf{R}\times\mathbf{I})\cdot[\mathbf{I}\times(\mathbf{B}\times\mathbf{I})]}{I^2B\sin\gamma},$$

$\mathbf{R}\times\mathbf{I}$ is the Hall field, $\mathbf{R}$ the Hall vector, γ the angle between $\mathbf{B}$ and $\mathbf{I}$. Using the vector identities

$$(\mathbf{a}\times\mathbf{b})\cdot(\mathbf{c}\times\mathbf{d})=\begin{vmatrix}\mathbf{a}\cdot\mathbf{c} & \mathbf{a}\cdot\mathbf{d}\\ \mathbf{b}\cdot\mathbf{c} & \mathbf{b}\cdot\mathbf{d}\end{vmatrix}\quad\text{and}\quad \mathbf{a}\times(\mathbf{b}\times\mathbf{c})=\mathbf{b}(\mathbf{a}\cdot\mathbf{c})-\mathbf{c}(\mathbf{a}\cdot\mathbf{b}),$$

we get: $\tilde{E}_{B\times I}=R_{I\times(B\times I)}I$ and $\tilde{E}_{I\times(B\times I)}=-R_{B\times I}I$, where $R_{I\times(B\times I)}$ and $R_{B\times I}$ are projections of the Hall vector $\mathbf{R}$ on unit vectors in the directions indicated by the subscripts and I is the magnitude of the current density.

APPENDIX B

Consider a crystallographic reference frame in which the axes are defined by: x_1—[100], x_2—[010], x_3—[001]. Suppose $\mathbf{B}$ is in the (001) plane and makes an angle α, reckoned positive if counterclockwise, with the 1-axis as shown in Fig. 13. The permissible form of $\tilde{\rho}_{ij}(\alpha)$ with respect to the crystallographic frame is:

$$\tilde{\rho}_{ij}(\alpha)=\begin{bmatrix}0 & 0 & -\tilde{\rho}_{13}(\alpha)\\ 0 & 0 & \tilde{\rho}_{23}(\alpha)\\ \tilde{\rho}_{13}(\alpha) & -\tilde{\rho}_{23}(\alpha) & 0\end{bmatrix}. \tag{14}$$

The angle which the magnetic field makes with the 1 axis is given in parenthesis. Because the 1 axis is a rotational axis of even order $\tilde{\rho}_{ij}(-\alpha)$ can be expressed in terms of $\tilde{\rho}_{ij}(\alpha)$ (only the sub-group of the 2-fold rotation is used) and

$$\tilde{\rho}_{ij}(-\alpha)=s_{im}s_{jn}\tilde{\rho}_{mn}(\alpha),$$

where

$$s_{ij}=\begin{bmatrix}1 & 0 & 0\\ 0 & -1 & 0\\ 0 & 0 & -1\end{bmatrix}.$$

Thus:

$$\tilde{\rho}_{ij}(-\alpha)=\begin{bmatrix}0 & 0 & \tilde{\rho}_{13}(\alpha)\\ 0 & 0 & \tilde{\rho}_{23}(\alpha)\\ -\tilde{\rho}_{13}(\alpha) & -\tilde{\rho}_{23}(\alpha) & 0\end{bmatrix}. \tag{15}$$

If $\mathbf{I}=(0,0,I_3)$ and if we transform (14) and (15) to laboratory frames:

$$E=[A\tilde{\rho}(\alpha)A^{-1}]I,$$

where

$$A=\begin{bmatrix}\cos\alpha & \sin\alpha & 0\\ -\sin\alpha & \cos\alpha & 0\\ 0 & 0 & 1\end{bmatrix},$$

we find $\hat{E}_B(\alpha)=-E_B(-\alpha)$. The particular geometry used in the proof is selected for convenience and is not essential. The result is valid in the plane formed by $\mathbf{B}$ and even-fold axis for an arbitrary direction of $\mathbf{B}$.

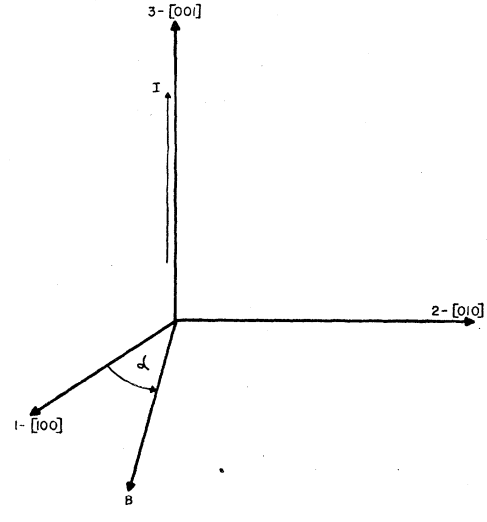

FIG. 13. Direction of $\mathbf{B}$ and $\mathbf{I}$ with respect to crystallographic axis. $\mathbf{B}$ is in (001) plane. See Appendix B.

APPENDIX C

For case a [see Fig. 2(a)] Eq. (11) yields:

$$\bar{L}_{11}=(1/3m_{11})[(2K+1)(2\sigma_{111}^{(1)}+\sigma_{\bar{1}11}^{(1)}+\sigma_{1\bar{1}1}^{(1)})+\tfrac{3}{2}K\omega^2\sin^2\theta(2\sigma_{111}^{(3)}+\sigma_{\bar{1}11}^{(3)}+\sigma_{1\bar{1}1}^{(3)})],$$

$$\bar{L}_{12}=(1/3m_{11})[(K-1)(-2\sigma_{111}^{(1)}+\sigma_{\bar{1}11}^{(1)}+\sigma_{1\bar{1}1}^{(1)})-\tfrac{3}{2}K\omega^2\sin^2\theta(2\sigma_{111}^{(3)}+\sigma_{\bar{1}11}^{(3)}+\sigma_{1\bar{1}1}^{(3)})],$$

$$\bar{L}_{13}=(1/3m_{11})[(K-1)(\sigma_{\bar{1}11}^{(1)}-\sigma_{1\bar{1}1}^{(1)})+(3/2\sqrt{2})K\omega^2\sin 2\theta(2\sigma_{111}^{(3)}+\sigma_{\bar{1}11}^{(3)}+\sigma_{1\bar{1}1}^{(3)})],$$

$$\bar{L}_{22}=\bar{L}_{11},$$

$$\bar{L}_{23}=\bar{L}_{13},$$

$$\bar{L}_{33}=(1/3m_{11})[(2K+1)(2\sigma_{111}^{(1)}+\sigma_{\bar{1}11}^{(1)}+\sigma_{1\bar{1}1}^{(1)})+3K\omega^2\cos^2\theta(2\sigma_{111}^{(3)}+\sigma_{\bar{1}11}^{(3)}+\sigma_{1\bar{1}1}^{(3)})], \quad (16)$$

$$\tilde{L}_{12}=-[\omega/3(m_{11}m_1)^{\frac{1}{2}}]\times[(K+2)\cos\theta(2\sigma_{111}^{(2)}+\sigma_{\bar{1}11}^{(2)}+\sigma_{1\bar{1}1}^{(2)})-\sqrt{2}(K-1)\cos\theta(\sigma_{\bar{1}11}^{(2)}-\sigma_{1\bar{1}1}^{(2)})],$$

$$\tilde{L}_{13}=-[\omega/3(m_{11}m_1)^{\frac{1}{2}}]\times\{(\sin\theta/\sqrt{2})[6\sigma_{111}^{(2)}+(2K+1)(\sigma_{\bar{1}11}^{(2)}+\sigma_{1\bar{1}1}^{(2)})]-(K-1)\cos\theta(\sigma_{\bar{1}11}^{(2)}-\sigma_{1\bar{1}1}^{(2)})\},$$

$$\tilde{L}_{23}=\tilde{L}_{13}.$$

Case b [see Fig. 2(b)] is calculated in reference 10 and is given below. ϕ' is defined in Fig. 2(b). Note that the LH-field $\tilde{E}_B{}^{\phi}$ calculated from (17), Eq. (13), is given in terms of the measured angle ϕ rather than ϕ'.

$$\bar{L}_{11}=(2/3m_{11})[(2K+1)(\sigma_{111}^{(1)}+\sigma_{\bar{1}\bar{1}1}^{(1)})],$$

$$\bar{L}_{23}=-(2/3m_{11})[(K+1)(\sigma_{111}^{(1)}-\sigma_{\bar{1}\bar{1}1}^{(1)})-K\omega^2\sin 2\phi'(\sigma_{111}^{(3)}+\sigma_{\bar{1}\bar{1}1}^{(3)})],$$

$$\bar{L}_{22}=(2/3m_{11})[(2K+1)(\sigma_{111}^{(1)}+\sigma_{\bar{1}\bar{1}1}^{(1)})+2K\omega^2\sin\phi'(\sigma_{111}^{(3)}+\sigma_{\bar{1}\bar{1}1}^{(3)})],$$

$$\bar{L}_{33}=(2/3m_{11})[(2K+1)(\sigma_{111}^{(1)}+\sigma_{\bar{1}\bar{1}1}^{(1)})+2K\omega^2\cos\phi'(\sigma_{111}^{(3)}+\sigma_{\bar{1}\bar{1}1}^{(3)})], \quad (17)$$

$$\bar{L}_{12}=\bar{L}_{13}=0,$$

$$\tilde{L}_{12}=-\tfrac{2}{3}[\omega/(m_{11}m_1)^{\frac{1}{2}}][(K+2)\cos\phi'(\sigma_{111}^{(2)}+\sigma_{\bar{1}\bar{1}1}^{(2)})-(K-1)\sin\phi'(\sigma_{111}^{(2)}-\sigma_{\bar{1}\bar{1}1}^{(2)})],$$

$$\tilde{L}_{13}=-\tfrac{2}{3}[\omega/(m_{11}m_1)^{\frac{1}{2}}][(K+2)\sin\phi'(\sigma_{111}^{(2)}+\sigma_{\bar{1}\bar{1}1}^{(2)})-(K-1)\cos\phi'(\sigma_{111}^{(2)}-\sigma_{\bar{1}\bar{1}1}^{(2)})],$$

$$\tilde{L}_{23}=0,$$

$\mathfrak{L}_{ij}=-\frac{2}{3}e^2L_{ij}$ is the conductivity tensor, m_{11} and m_1 are the longitudinal and transverse effective masses, $K=m_{11}/m_1$, $\omega=eB/(m_{11}m_1)^{\frac{1}{2}}c$. Equations (16) and (17) are written in a crystallographic frame of reference.

APPENDIX D

The geometry of the sample is shown in Figure 5 and its position with respect to the magnetic field in Fig. 14. We assume that the voltages $\tilde{V}_{P1}$ and $\tilde{V}_{P2}$ are proportional to the electric fields in the directions P_1-P_1 and P_2-P_2 in a long thin sample without arms cut in the same manner with respect to the crystallographic

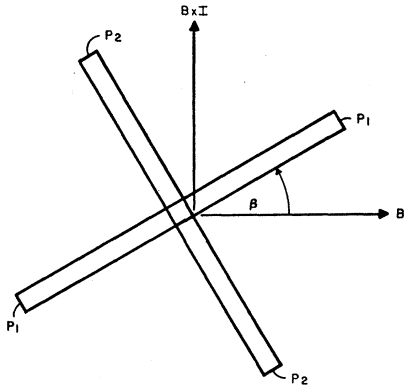

FIG. 14. Top view of "three dimensional cross" (see Fig. 5). Current leg perpendicular to plane of paper. Potential probes P_1, P_2, and **B** in plane of paper. P_1 makes an angle β with B.

axes as the current leg of Fig. 14. Further, we assume that the proportionality factors are identical. Then

$$\tilde{V}_{P1}=\tilde{V}_B\cos\beta+\tilde{V}_{B\times I}\sin\beta,$$

$$\tilde{V}_{P2}=\tilde{V}_B\sin\beta+\tilde{V}_{B\times I}\cos\beta$$

$\tilde{V}_B$ and $\tilde{V}_{B\times I}$ are the line integrals of the electric field along imaginary arms parallel to **B** and **B**×**I** and equal in length to those on the sample. Clearly $(\tilde{V}_{P1}/\tilde{V}_{P2})_{B\to 0}=\tan\beta$ because of Eqs. (9) and (10). This method for determining β works only for materials crystallizing in the cubic system because it is only for such materials that the linear term in the expansion of $\tilde{E}_B$ with respect to **B** vanishes. In practice $\tilde{V}_{P1}/\tilde{V}_{P2}$ is plotted *versus* B^2 and extrapolated to zero giving $\tan\beta$. $\tilde{V}_B$ and $\tilde{V}_{B\times 1}$ are then determined for arbitrary fields from the expressions.

$$\tilde{V}_B=\tilde{V}_{P1}\cos\beta-\tilde{V}_{P2}\sin\beta,$$

$$\tilde{V}_{B\times I}=\tilde{V}_{P1}\sin\beta+\tilde{V}_{P2}\cos\beta.$$